

Supramolecular Mechanism of Viral Envelope Disruption by Molecular Tweezers

Tatjana Weil,[▲] Rüdiger Groß,[▲] Annika Röcker,[▲] Kenny Bravo-Rodriguez,[▲] Christian Heid, Andrea Sowislok, My-Hue Le, Nelli Erwin, Mridula Dwivedi, Stephen M. Bart, Paul Bates, Lukas Wettstein, Janis A. Müller, Mirja Harms, Konstantin Sparrer, Yasser B. Ruiz-Blanco, Christina M. Stürzel, Jens von Einem, Sina Lippold, Clarissa Read, Paul Walther, Marco Hebel, Florian Kreppel, Frank-Gerrit Klärner, Gal Bitan, Michael Ehrmann, Tanja Weil, Roland Winter, Thomas Schrader,* James Shorter,* Elsa Sanchez-Garcia,* and Jan Münch*



Cite This: *J. Am. Chem. Soc.* 2020, 142, 17024–17038



Read Online

ACCESS |



Metrics & More

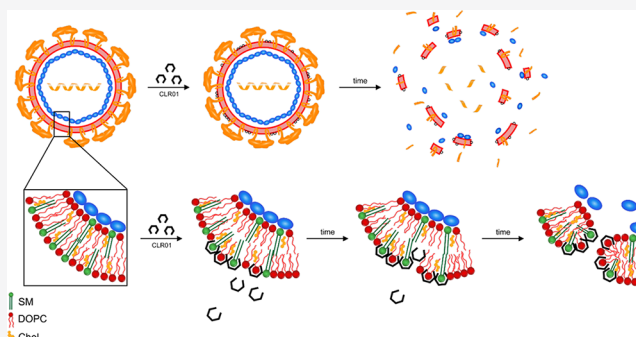


Article Recommendations



Supporting Information

ABSTRACT: Broad-spectrum antivirals are powerful weapons against dangerous viruses where no specific therapy exists, as in the case of the ongoing SARS-CoV-2 pandemic. We discovered that a lysine- and arginine-specific supramolecular ligand (CLR01) destroys enveloped viruses, including HIV, Ebola, and Zika virus, and remodels amyloid fibrils in semen that promote viral infection. Yet, it is unknown how CLR01 exerts these two distinct therapeutic activities. Here, we delineate a novel mechanism of antiviral activity by studying the activity of tweezer variants: the “phosphate tweezer” CLR01, a “carboxylate tweezer” CLR05, and a “phosphate clip” PC. Lysine complexation inside the tweezer cavity is needed to antagonize amyloidogenesis and is only achieved by CLR01. Importantly, CLR01 and CLR05 but not PC form closed inclusion complexes with lipid head groups of viral membranes, thereby altering lipid orientation and increasing surface tension. This process disrupts viral envelopes and diminishes infectivity but leaves cellular membranes intact. Consequently, CLR01 and CLR05 display broad antiviral activity against all enveloped viruses tested, including herpesviruses, Measles virus, influenza, and SARS-CoV-2. Based on our mechanistic insights, we potentiated the antiviral, membrane-disrupting activity of CLR01 by introducing aliphatic ester arms into each phosphate group to act as lipid anchors that promote membrane targeting. The most potent ester modifications harbored unbranched C4 units, which engendered tweezers that were approximately one order of magnitude more effective than CLR01 and nontoxic. Thus, we establish the mechanistic basis of viral envelope disruption by specific tweezers and establish a new class of potential broad-spectrum antivirals with enhanced activity.



INTRODUCTION

Classical therapeutic strategies against viral infections focus primarily on inhibiting viral replication; in a “one bug—one drug” concept, a specific protease and polymerase inhibitor is developed for each virus. However, for an increasing number of new viruses, no treatment is available, and there is an urgent need for innovation. A new approach has recently emerged which targets the virions themselves. This strategy has the potential to achieve broad antiviral activities especially against the constant threat of zoonoses, which are a major issue as evidenced by the newly emerged coronavirus, SARS-CoV-2. It involves external interference with the membrane fusion process which is essential for all enveloped viruses.^{1,2} Major avenues comprise inhibition of fusion proteins³ (e.g., by antiviral peptides [AVPs]⁴ or protein disulfide isomerase [PDI] inhibitors⁵) and modulation of membrane properties such as

integrity (e.g., by virolytic peptides⁶), fluidity (e.g., by polyunsaturated ER-targeting liposomes [PERLs]⁷), or curvature (e.g., by rigid amphipathic fusion inhibitors [RAFIs]⁸). Finally, membrane properties essential for fusion are influenced by lipid oxidation which can be brought about by type II photosensitizers that oxidize unsaturated phospholipids (e.g., certain amphiphilic thiazolidines⁹). The “molecular tweezers” described in this work also modulate membrane integrity, albeit in a very subtle way: they specifically recognize lipid head groups

Received: June 12, 2020

Published: September 14, 2020



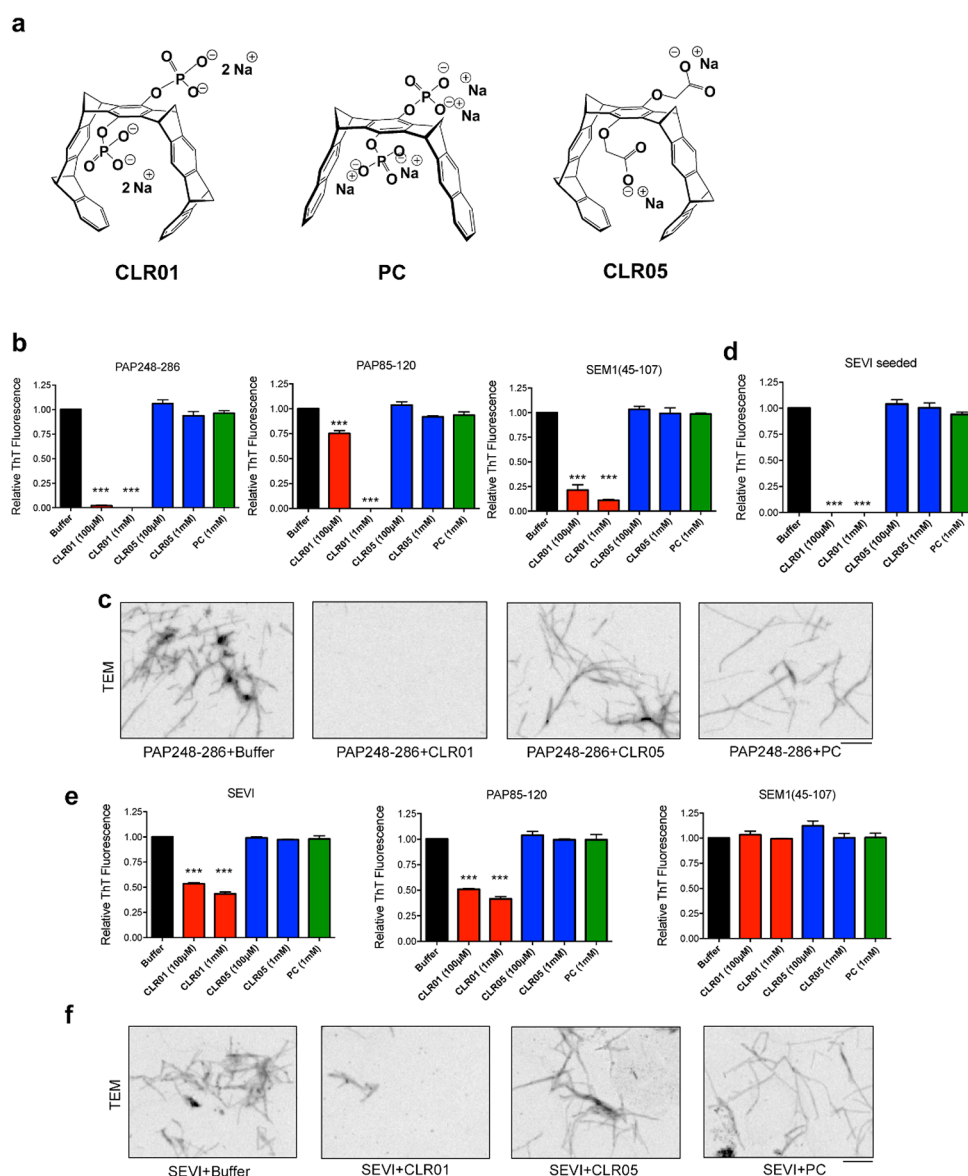


Figure 1. The molecular tweezer CLR05 and the clip PC neither inhibit amyloid assembly nor remodel amyloid fibrils. (a) Chemical structures of the hydrogen phosphate tweezer CLR01, methylene carboxylate tweezer CLR05, and the naphthalene phosphate clip PC. (b, c) CLR05 and PC do not inhibit amyloid fibril formation. (b) PAP248–286 (1 mM), PAP85–120 (1 mM), and SEM1(45–107) (0.5 mM) peptides were incubated with the indicated concentrations of CLR01, CLR05, PC, or buffer and agitated at 1400 rpm at 37 °C. After 24 h (PAP85–120) or 72 h (PAP248–286 and SEM1(45–107)), fibrillization was assessed using the amyloid-binding dye Thioflavin-T (ThT). Values represent means \pm SEM ($n = 3$). (c) PAP248–286 (1 mM) was incubated with CLR01 (1 mM), CLR05 (1 mM), PC (1 mM), or buffer and agitated at 1400 rpm at 37 °C. After 72 h, fibrillization was assessed by transmission electron microscopy (TEM). Bar, 250 nm. (d) PAP248–286 (1 mM, plus 2 wt %/wt SEVI fibrils) was incubated with the indicated concentrations of CLR01, CLR05, PC, or buffer and agitated at 1400 rpm at 37 °C. After 48 h, fibrillization was assessed using the amyloid-binding dye Thioflavin-T (ThT). Values represent means \pm SEM ($n = 3$). (e) CLR05 and PC do not remodel preformed fibrils. SEVI, PAP85–120 fibrils, or SEM1(45–107) fibrils (20 μ M) were incubated with the indicated concentrations of CLR01, CLR05, or PC. After 2 h at 37 °C, ThT fluorescence was measured. Values represent means \pm SEM ($n = 3$). (f) SEVI fibrils (20 μ M) were incubated with CLR01 (1 mM), CLR05 (1 mM), or PC (1 mM). After 2 h at 37 °C, reactions were processed for TEM. Bar, 250 nm. For b, d, and e, one-way ANOVA (nonparametric, grouped) and Dunnett’s multiple comparison tests were applied to compare the compound-treated samples to the respective buffer control.

and increase surface tension—a truly supramolecular mechanism which operates on all enveloped viruses. The molecular tweezer CLR01 (Figure 1a) is an inhibitor of aggregation and toxicity of amyloidogenic polypeptides containing arginine or lysine residues.^{10–13} Through specific binding to lysine and arginine residues, CLR01 prevents polypeptide assembly into amyloid and even remodels mature fibrils.¹² We established that CLR01 also inhibits the assembly of seminal amyloids formed by specific proteolytic fragments of prostatic acid phosphatase (PAP) and semenogelins (SEM).¹⁴ These fibrils are naturally

present in human semen and markedly enhance the infectivity of sexually transmitted viruses such as human immunodeficiency virus type 1 (HIV-1),^{15–19} herpesviruses,²⁰ and Ebola virus (EBOV).²¹ CLR01 also remodels preformed PAP248–286 fibrils (termed SEVI for semen-derived enhancer of virus infection) and PAP85–120 fibrils.¹⁴ Semen amyloids are polycationic due to several arginine and lysine residues and bind to the negatively charged membranes of viral particles and cells, which increases viral attachment and augments fusion.^{15,17,22,23} Unexpectedly, we previously found that

CLR01 not only antagonizes the infectivity-enhancing activity of seminal amyloids but also exerts a direct antiviral activity against several enveloped viruses such as HIV-1, hepatitis c virus (HCV), herpes simplex virus type 2 (HSV-2), human cytomegalovirus (HCMV), Zika virus (ZIKV), and Ebola virus.^{14,24} The antiviral activity is a consequence of the direct interaction of CLR01 with the membrane of the enveloped viral particle, which ultimately results in the loss of virion integrity and hence infectivity.^{14,24} However, the precise antiviral mechanism of CLR01 remains unclear.

Due to their broad antiviral activity, CLR01 and its enhanced variants defined here are promising leads for the development of a new class of potential antiviral drugs that specifically destroy the structural integrity of enveloped viruses.^{14,24} Yet, although it is essential for future therapeutic applications, the underlying mechanism of viral membrane destabilization is still unknown.¹⁴ To address this issue and to identify the structural requirements for suppressing amyloid formation, we investigated how molecular tweezers, and a related clip-like molecule with known supramolecular behavior, affect amyloidogenesis and viral membrane integrity. In addition to the “phosphate tweezer” CLR01, we analyzed the “carboxylate tweezer” CLR05 and the “phosphate clip” PC (Figure 1a). These three scaffolds were selected for this mechanistic study because they represent prototypes that display different binding profiles. Tweezers with phosphate, phosphonate, or sulfate anions behave very similarly, but CLR01 is the least toxic among them. The carboxylate tweezer, CLR05, has a cavity (Figure 1a) but displays reduced affinity for lysine or arginine, and thus, we hypothesized it might have reduced ability to antagonize protein aggregation. The phosphate clip, PC, differs from CLR01 only in its cavity shape, which is more open due to the planar naphthalene side walls (Figure 1a). With these characteristic supramolecular host structures, we hoped to probe and separate the different mechanistic paths of antiviral and anti-amyloid action. Using a synergistic approach combining computational chemistry, cell biology, virology, supramolecular binding studies, and biophysics, we elucidated both the anti-amyloid and antiviral mechanisms. We found that lysine complexation inside the tweezer cavity is required to antagonize amyloidogenesis. The formation of inclusion complexes with lipid head groups of the viral membrane increases surface tension and disrupts the viral membrane, resulting in diminished infectivity. Our findings explain the origin of viral envelope destabilization by tweezers. With the identification of CLR05 as an antiviral agent, in addition to CLR01, we establish these supramolecular ligands as a new class of broadly active antiviral compounds. Based on these mechanistic insights, a series of advanced new tweezer derivatives was designed with additional lipid anchors. These novel tweezers exhibited potentiated antiviral activity compared to the parental CLR01 scaffold.

RESULTS

CLR05 and PC Have No Anti-amyloid Activity. To define the mechanism of CLR01 action, we first established the activity of CLR05 and PC. The tweezers (CLR01 and CLR05) and the clip (PC) share the same central unit but carry distinct sidewalls, which form cavities with typical shapes, thus enabling their specific binding profiles (Figure 1a, Table 1). CLR01 forms inclusion complexes with lysine residues and to a lesser extent with arginine.²⁵ CLR05 is structurally similar to CLR01, but the hydrogen phosphate substituents are replaced with methylene carboxylate groups (Figure 1a). The phosphate clip, PC, with its

Table 1. Lysine and Arginine Affinities of the Three Host Molecules (CLR01, CLR05, and PC) Determined by Fluorescence Titrations in 75 mM Phosphate Buffer (pH 7.4)

host	K_d (μ M) Ac-Lys-OMe	Ac-Arg-OMe
CLR01 ²⁵	17	22
PC ²⁹	4670	1760
CLR05 ²⁵	1160	1390

almost parallel naphthalene sidewalls, was designed for planar aromatic guests such as cationic cofactors, which are preferentially accommodated inside its cavity^{26,27} (Figure 1a). In sharp contrast, inclusion of aliphatic cationic guests such as Lys or Arg inside PC is less favored and occurs only with low affinity²⁸ (Table 1).

In solution, CLR05 forms both chelates and inclusion complexes with Lys/Arg residues²⁵ (Supplementary Figure 1a). However, it is important to clarify CLR05 behavior in a protein environment. In line with its experimentally determined low Lys and Arg affinities in solution²⁵ (Table 1), our computational studies of the CLR05 interaction with the prototype amyloidogenic peptide in semen, PAP248–286, showed that CLR05 has a reduced ability to form inclusion complexes with Lys or Arg, as compared to CLR01 (Supplementary Figures 1b and 1d). The global minima on the peptide-tweezer free energy surfaces obtained with extended-system adaptive biasing force (eABF) calculations indicate that binding of CLR05 to residues at the N-terminal (K251) and C-terminal (K281 and K282) regions of PAP248–286 is not favored, whereas K253 and R257 form distorted, unstable inclusion complexes (Supplementary Figure 1b and 1c). In addition, free energy perturbation calculations indicate that CLR01 forms more stable inclusion complexes with almost all Lys or Arg residues in PAP248–286, as compared to CLR05 (Supplementary Figure 1d). The only exception was R273, which formed a more stable inclusion complex with CLR05 than with CLR01 (Supplementary Figure 1d). However, R273 is not located in any of the hexapeptides predicted to form self-complementary β -sheets, termed steric zippers, which are anticipated to contribute to SEVI fibril formation.^{14,19} Importantly, unlike CLR01,¹⁴ CLR05 fails to interact effectively with K281 and K282, which are located in two potent steric zippers at the C-terminal end of PAP248–286¹⁹ and form part of the stable cross- β SEVI fibril core defined by hydrogen–deuterium exchange.³⁰ Collectively, these findings predict that CLR05 would lack the anti-amyloid activity of CLR01. Similarly, we expected that PC would not show anti-amyloid activity because its affinity for Lys/Arg is even lower than that of CLR05 (Table 1).

For the experimental evaluation of these predictions, we investigated the effects of CLR01, CLR05, and PC on the formation of semen amyloid fibrils. Indeed, unlike CLR01, neither CLR05 nor PC inhibit spontaneous assembly of PAP248–286, PAP85–120, and SEM1(45–107) fibrils (Figure 1b, c). Moreover, CLR05 and PC did not inhibit fibrillization of PAP248–286 that was seeded by preformed SEVI fibrils (Figure 1d). Likewise, CLR05 and PC were unable to remodel preformed SEVI or PAP85–120 fibrils (Figure 1e, f), and none of the scaffolds could remodel SEM1(45–107) fibrils (Figure 1e).¹⁴ Thus, in contrast to CLR01, CLR05 has no anti-amyloid activity. As expected, due to its architecture, PC does not bind aliphatic guests and did not affect fibril formation by any of the peptides.

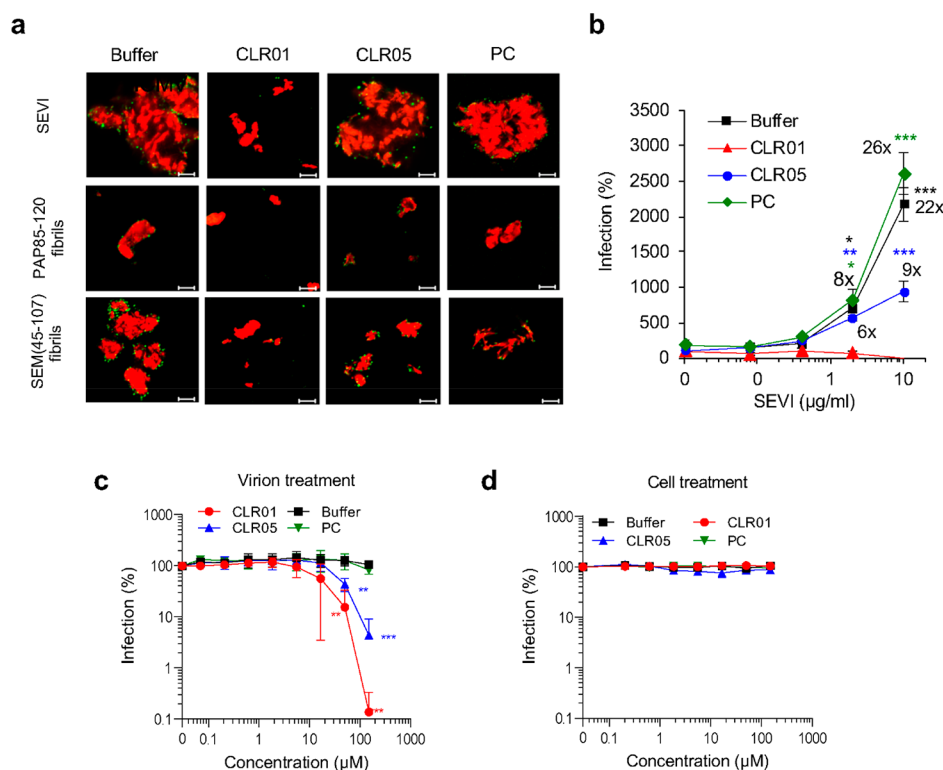


Figure 2. CLR05 anti-HIV-1 activity. (a) CLR05 and PC do not prevent formation of virus-fibril complexes. Fibrils (200 μg/mL) were incubated with buffer, CLR01, CLR05 or PC in 20-fold molar excess for 5 min and stained with Proteostat Amyloid Plaque Detection Kit. MLV-Gag-YFP particles (green) were added 1:2 and incubated with the stained fibrils (red) for 5 min before samples were analyzed via confocal microscopy. Scale bar: 5 μm. (b) CLR05 but not PC decreases the HIV-1 enhancing activity of SEVI. Fibrils were incubated with buffer or a 20-fold molar excess of CLR01, CLR05 or PC for 10 min at room temperature. After preparing 5-fold dilution series of the mixtures, HIV-1 was added and TZM-bl cells were inoculated with these samples. Values represent % β-galactosidase activities (mean) compared to cells infected with virus only and are obtained from triplicate infections ± SEM (*n* = 9). Numbers above the symbols indicate *n*-fold enhancement of infection. (c, d) CLR05 blocks HIV-1 infection by targeting the virus. (c) HIV-1 was incubated with CLR01, CLR05, PC or buffer for 10 min at 37 °C before it was added to TZM-bl cells. Three days post infection (dpi), infection rates were quantified by measuring β-galactosidase activity in cellular lysates. Values represent % infection (mean) compared to buffer control ± SD (*n* = 3). (d) TZM-bl cells were incubated with the indicated concentrations of CLR01, CLR05, PC or buffer for 1 h at 37 °C. Cell supernatants were discarded, and cells were infected with CCR5-tropic HIV-1 NL4–3. Values represent % infection (mean) compared to buffer control ± SD (*n* = 3).

CLR05 and PC Do Not Prevent the Formation of Virus–Fibril Complexes nor Abrogate Viral Infection Enhancement. CLR01 not only has anti-amyloid activity but also prevents the formation of complexes between seminal fibrils and HIV-1 particles.¹⁴ In contrast, we discovered that CLR05 and PC do not inhibit complexation of YFP-tagged virions with the three types of seminal amyloids (Figure 2a). We next determined the effect of CLR05 and PC on cell growth and found that concentrations of up to 250 μM were well-tolerated (Supplementary Figure 2a). Thus, all subsequent experiments were performed with CLR05 and PC concentrations ≤150 μM to exclude any confounding effects caused by residual cytotoxicity. To determine the effect of CLR05 and PC on amyloid-mediated infectivity enhancement, SEVI fibrils were incubated with PBS or with a 20-fold molar excess of each tweezer/clip, then mixed with HIV-1 and this solution was used to inoculate target cells. SEVI fibrils increased HIV-1 infection in a dose-dependent manner as described previously,¹⁵ and CLR01 eradicated this effect¹⁴ (Figure 2b). In the presence of CLR05, however, the infectivity enhancing activity of the fibrils was reduced but not abrogated. PC was completely inactive in antagonizing the infection enhancing effects of SEVI (Figure 2b). The experiment was also performed with PAP85–120 and SEM1(45–107) fibrils. Again, CLR01 abrogated infectivity

enhancement, CLR05 showed an intermediate effect and PC was inactive (Supplementary Figure 2b–d). Since CLR05 has no anti-amyloid activity (Figure 1b–1d), these data suggest that reduced infection rates are due to a direct antiviral activity of CLR05.

CLR05 has direct anti-HIV activity. Next, we tested CLR01, CLR05 and PC for a direct effect on virus infection. First, HIV-1 particles were incubated with tweezers, clip or buffer, and then used for infection. PC did not exert any antiviral activity whereas CLR05 inhibited HIV-1 infection with a half-maximal inhibitory concentration (IC₅₀) of ~41 μM, which is ~2.4-fold higher than the IC₅₀ of CLR01 (~17 μM) (Figure 2c, Supplementary Figure 2e). Like CLR01, CLR05 did not inhibit HIV-1 infection if target cells were pre-exposed to the tweezer, demonstrating that both tweezers target the virus itself (Figure 2d).

Tweezers and clip form inclusion complexes with lipid head groups. To understand the antiviral effects of CLR01 and CLR05 at the molecular level, we investigated if the tweezers and the clip directly interact with the lipid head groups in the viral envelope, first by molecular dynamics simulations, then by NMR titration. The composition of viral envelopes greatly varies with the type of virus, the host cell membrane and the cell type. Generally, however, viral membranes tend to be enriched in

lipids found in lipid rafts (lipid microdomains enriched in glycosphingolipids and cholesterol) such as sphingomyelin (SM),^{31,32} because viruses bud directly from lipid-raft domains of cell membranes.³³ Thus, lipidomics analyses provide experimental evidence of a special enrichment of HIV-1 viral membranes in SM and Cholesterol (Chol), phosphatidylserine (PS) and plasmalogen-phosphatidylethanolamine (pl-PE), all leading to more rigid membranes characteristic of lipid rafts.³¹ A similar case can be made for the influenza virus, which is likewise enriched in SLs (sphingolipids) and cholesterol, irrespective of the investigated producer cell line.³² Thus, viral membranes tend to resemble the lipid-raft microdomains from whence they originate.^{31,34–37}

For our calculations, we selected three abundant lipids which occur in both eukaryotic cells and virions: dipalmitoylphosphatidylcholine (DOPC), sphingomyelin (SM) and cholesterol (Chol). To account for the different degree of lipid rafts, we composed a simple bilayer containing 120 DOPC lipids per leaflet, and a mixed bilayer containing 54, 30, and 36 molecules per leaflet of DOPC, sphingomyelin (SM) and cholesterol (Chol), respectively. We then studied the interaction of CLR01, CLR05 and PC with these model membranes using unbiased molecular dynamics simulations. Our simulations contained nine molecules of tweezers or clip, initially placed 4 Å above the membrane (example shown for CLR01 in Supplementary Figure 3a). Our results indicate that CLR01, CLR05 and PC form inclusion complexes with the head groups of DOPC and SM lipids, in both the DOPC and the mixed bilayer (Supplementary Tables 1–4, Supplementary Figures 4a–c). Importantly, after forming an inclusion complex, CLR01 and CLR05 induce preferential orientations of the complexed lipid head groups (Figure 3a and 3b), unlike PC (Figure 3a and 3c). Upon inclusion inside CLR01 or CLR05, the lipid head groups adopt an orientation nearly perpendicular to the normal of the membrane (z -axis) (the angle with respect to the z -axis is $\sim 90^\circ$, Figure 3b). This distortion is dictated by the upright orientation of the amphiphilic tweezer inside the membrane whose cavity must be entered from the side. Consequently, the whole tweezer is inserted in the most external layer of the membrane, formed by the polar ammonium and phosphate groups of its phospholipid components (Figure 3b). This tweezer orientation likely induces local stress around the binding site thus weakening the bilayer. By contrast, in the presence of PC, the lipid head group remains aligned nearly parallel to the normal of the membrane (z -axis) (Figure 3c). This alignment can occur because the clip cavity is more open than the tweezer cavity, which enables facile lipid inclusion into the clip cavity by vertical entry.

To further explore the finding that the tweezers encapsulate lipid head groups and do not penetrate into the membrane interior, the free energy changes for the insertion of CLR01, CLR05 and PC into a DOPC or a mixed bilayer were calculated using the eABF scheme (Supplementary Figure 3 shows CLR01 as a representative case). For both bilayers, the minimum in the one-dimensional Potential of Mean Force (PMF) profile corresponds to the tweezers forming an inclusion complex with a head group of a lipid located at the surface of the membrane (as indicated by position 2 in Supplementary Figure 3b) rather than inside the bilayer where the free energy is much higher (position 3, Supplementary Figure 3b). Although the free energy differences between the tweezers in solution (position 1, Supplementary Figure 3b) and the complex at the surface of the membrane (position 2, Supplementary 3b) are very small, the MD simulations indicate that the tweezer-lipid complexes do

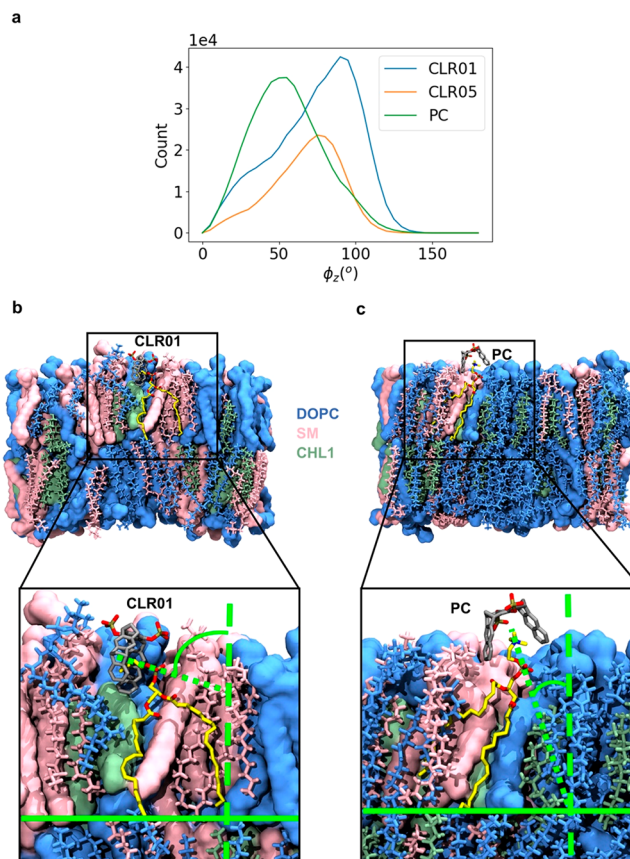


Figure 3. Computational modeling of the interactions of the tweezers and clip with lipid membranes. (a) The distribution of the values adopted by the angle indicating the relative orientation of the lipid head group with respect to the normal of the membrane model (z axis) provides evidence that the orientations of the lipids are different upon interaction with the tweezers with respect to the clip. (b) Upon binding to a lipid in the bilayer, the tweezers (CLR01 is shown here as representative case) enforce a conformation of the lipid head group almost parallel to the bilayer surface, raising surface tension. (c) By contrast, the lipid head group bound to PC remains nearly perpendicular to the bilayer surface in a tension-free conformation. An enlargement of the binding region is shown for both b) and c). CLR01 and PC are depicted as sticks with carbon atoms in gray, oxygen in red and phosphorus in tan. DOPC is shown in blue, PSM in pink and CHL1 in green. The lipid bound to CLR01 or PC is highlighted in yellow. The dotted line is traced along the vector between the centers of the phosphate and the ammonium groups in the lipid head. The solid line indicates the plane of the membrane and the dashed line corresponds to the direction of its normal vector (z -axis).

form, albeit not as efficiently as the PC–lipid complexes (Supplementary Table 1). Importantly, the free-energy calculations establish that CLR01, CLR05 and PC are unlikely to penetrate deep inside or cross the bilayers. The key to the antiviral activity of the tweezers most likely relates to their effect on the lipid orientation, as discussed above, and/or a preference of the tweezers toward lipids like SM, which are characteristic of viral membranes.

Here, to explore if CLR01 has a certain preference for raft-forming lipids, we performed quantum mechanics/molecular mechanics (QM/MM) calculations. Our results indicate that the CLR01-SM complex is indeed more stable (in terms of electronic energy) than the CLR01-DOPC complex (Supplementary computational details, Supplementary Figure 5a and 5b). To clarify if this selective stabilization of the CLR01-SM

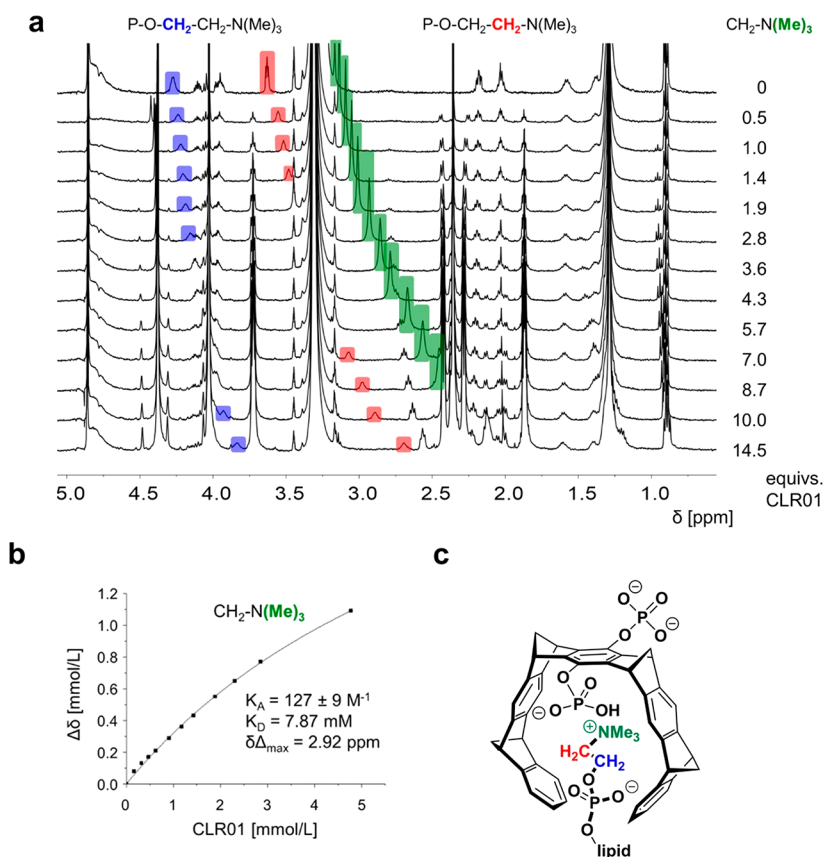


Figure 4. Tweezers and clip form inclusion complexes with lipid head groups. (a) Complex formation between CLR01 and sphingomyelin (SM) monitored by NMR spectroscopy: stacked plot of ^1H NMR spectra showing SM with increasing amounts of added CLR01. Colored signals represent the choline head group inserted into the tweezer cavity. (b) Corresponding binding curve for the $\text{N}(\text{Me})_3^+$ signal with the resulting affinity (K_A/K_D) and $\Delta\delta_{\text{max}}$ value obtained from nonlinear regression. (c) Lewis structure of CLR01 with inserted choline moiety from PSM inside; CH_2/CH_3 groups inside the tweezer cavity are color-coded because they undergo large upfield shifts.

complexes is related to the disruption of interactions between the lipid molecules and the solvent or due to the membrane environment, we also calculated CLR01-SM and CLR01-DOPC inclusion complexes in an explicit water environment using the same computational protocol as in the membrane simulations. We found that the CLR01-SM complex is more stable than the CLR01-DOPC complex also in solution (Supplementary Figure 5b). Our results suggest that the hydration of the lipid polar head groups is the main determinant of the higher affinity of the tweezers for SM. This finding can be rationalized by the fact that the lipid bilayer is commonly hydrated at its most external regions composed of quaternary ammonium and phosphate groups. The binding of the tweezers implies desolvation of the ammonium moiety and partial desolvation of the phosphate group of the lipid. Hence, the stabilization of the inclusion complex is determined by competing forces between electrostatic and dispersion interactions with the tweezers and the solvation of the polar groups of the lipid. Notably, the phosphate group of SM establishes a stabilizing intramolecular hydrogen bond with the hydroxyl group next to it (Supplementary Figure 5c), unlike DOPC. This interaction diminishes the desolvation cost in SM thereby stabilizing the CLR01-SM complex. Conversely, the DOPC molecules depend completely on the surrounding water to stabilize the phosphate group, resulting in a higher desolvation cost for the formation of CLR01-DOPC inclusion complexes. Although lipid rafts are composed of various different rigid lipids, such effects may contribute to a preferred complexation of prominent raft lipids by the tweezers,

and contribute to their low toxicity toward cells relative to enveloped viruses. Taken together, our modeling experiments suggest an explanation for the preferential destabilization of viral membranes by molecular tweezers: they reveal that lipid head groups are included in the tweezer cavity, which causes alterations in lipid orientation that destabilize the membrane. Indeed, the formation of a supramolecular complex allows for the insertion of the tweezers in the hydrophilic region of the outer membrane leaflet. Consequently, membrane tension will increase in both cellular and viral membranes. However, if viral membranes are enriched in lipid rafts, this effect will elevate their tension above a tolerable threshold and lead to membrane rupture.

NMR titrations corroborate the formation of inclusion complexes with lipids. To complement the computational studies, we proceeded to structural investigations. ^1H NMR spectra of the 1:1 complexes (0.33 mM) between hosts (tweezers and clip) and lipids (SM, DOPC) revealed significant complexation-induced upfield shifts for the protons of the entire trimethylammonium choline head group, indicating at least partial inclusion inside the host cavities (Figure 4a). Figure 4 shows the example of phosphosphingomyelin interacting with CLR01. All the other combinations are presented in Supplementary Figures 6a-f. Attempted fluorescence titrations in methanol gave very small changes in host emission intensity, too small for reliable quantification. After careful optimization, a comparative NMR study was executed in d_4 methanol (due to the low lipid solubility in water), with all three host molecules

and DOPC as well as SM as guests. Binding isotherms produced excellent fits by nonlinear regression (Figure 4b) and revealed weak affinities resulting from K_d values in the low millimolar regime (Table 2). Maximum complexation-induced ^1H NMR

Table 2. Maximum Complexation-Induced Chemical ^1H NMR Shift Changes ($\Delta\delta_{\text{max}}$ [ppm]) of the $\text{N}(\text{Me})_3^+$ Protons and Dissociation Constants K_d Obtained From NMR Titrations of Lipids (PSM, DOPC) with Hosts (CLR01, CLR05, PC)^a

host	$\Delta\delta_{\text{max}}$ (ppm)		K_d (1:1)	
	SM	DOPC	SM (mM)	DOPC (mM)
CLR01	2.92	4.36	7.9	14
PC	0.89	1.45	7.0	13
CLR05	1.73	0.96	61	37

^aLipid concentration was 0.33 mM in d_4 -methanol.

chemical upfield shifts reached remarkable $\Delta\delta$ values of up to 4 ppm and demonstrated the efficient inclusion of the entire choline lipid head group inside the respective host cavities (Figure 4c).

We asked if the weak affinities originate from the steric bulk of the trimethylammonium head group and turned to trimethyllysine: NMR spectra for CLR01 with this related guest molecule reached comparable upfield shifts for the NMe_3^+ cation, but titrations maintained the high lysine affinity ($K_d \sim 10 \mu\text{M}$). We conclude that the close proximity between the choline phosphate ester anion and the anionic substituents of the tweezers or clip severely limits lipid affinities, whereas the extended alkylammonium arms of Lys or Arg fit well into the tweezer cavity, and most likely benefit from large dispersive and electrostatic attraction. CLR01 and PC produce comparable affinities toward both lipids (SM ~ 7 mM; DOPC ~ 14 mM) (Table 2). By contrast, CLR05 is a much weaker lipid binder (~ 40 – 60 mM), most likely because it also chelates the choline head group externally, as evidenced by the modest complexation-induced ^1H NMR upfield shifts compared to CLR01 (Figure 4, Supplementary Figure 6). This finding agrees well with poor lysine inclusion by CLR05²¹ and with the simulations (binding events and free energy calculations).

CLR05 Selectively Disrupts Raft-Rich Membranes. To further investigate the consequences of the tweezer/clip interaction with lipid bilayers, we took advantage of two types of engineered giant unilamellar vesicles (GUVs) of ~ 5 – $40 \mu\text{m}$ in diameter. In parallel with the calculations, one type of GUVs consisted only of DOPC. The other type of GUVs was composed of a 45/25/30 mol % mixture of DOPC, SM, and Chol as a membrane model with a large content of lipid rafts. These models are not intended to exactly recreate viral or eukaryotic cell membranes per se, whose lipid composition greatly varies and is much more complex. Instead, they aim at testing whether an elevated lipid raft content of representative lipids enriched in viral membranes renders them more susceptible to disruption by tweezers.

The different lipid phases were marked with fluorescent lipid analogs that segregated into the liquid-disordered (l_d) (red channel) or the liquid-ordered (l_o) (green channel) phase when viewed via fluorescence microscopy (Figure 5a and b). In addition, the GUVs were loaded with the water-soluble dye ATTO 647 (blue channel). Exposure of DOPC vesicles to CLR05 (Figure 5a, bottom panel) or PC (Figure 5b, bottom panel) did not affect vesicle morphology and did not elicit dye

leakage. However, when CLR05 was added to DOPC/SM/Chol vesicles, the l_o domains started to bud from the GUVs, and most of them had pinched off after ~ 15 – 30 min of incubation with concomitant dye leakage from the GUVs (Figure 5a, top panel). However, in contrast to CLR01, which destroys the mixed vesicles,¹⁴ CLR05 partially preserved GUV membrane integrity (Figure 5a, top panel). In sharp contrast, the clip did not permeabilize either of the GUV species even after 60 min of incubation (Figure 5b). Under identical conditions, CLR01 had a much more drastic effect: While the DOPC vesicles remained all intact, already after 5 min all membranes of mixed vesicles were disrupted, and the dye was lost completely.¹⁴

To study membrane disruption in the context of virus-like vesicles, mixed-lipid (DOPC/SM/Chol, 45/25/30 mol %) liposomes were prepared and loaded with carboxyfluorescein at a self-quenching concentration of 50 mM. In this setup, an increase in fluorescence indicates membrane disruption due to dye leakage and dilution below self-quenching concentrations in the surrounding medium. CLR05 and CLR01 but not PC induced dye leakage in a dose-dependent manner within few minutes (Figure 5c). CLR05 was less potent than CLR01 (Figure 5c). CLR01 rapidly induced full leakage of liposomes at 150 μM concentration, whereas CLR05 resulted in a maximal leakage of only 78% after 30 min of coincubation at the same concentration (Figure 5c, Supplementary Figure 7a). The previously reported antivirally inactive spacer molecule CLR03¹⁴ behaved similarly to PC and did not induce leakage (Supplementary Figure 7a–c).

Atomic force microscopy (AFM) of the heterogeneous model biomembrane confirmed that the line tension at the phase interface is increased in the presence of CLR05 (Figure 5d). As a result, the size of the l_o domains increased, which is accompanied by a slight increase in the difference in domain height thickness. This effect is likely due to an increased line tension at the boundary between the ordered and disordered domains induced by CLR05 attachment. AFM experiments demonstrated that addition of PC produced a small increase in height difference between the l_o and l_d phase as well; however, changes in the lateral membrane organization were small (Figure 5d). This finding further confirms that PC binds to the lipid bilayer although it does not disrupt it, pointing to a subtle but profound difference in its mode of action compared to the tweezers, CLR05 and CLR01, which disrupt membranes enriched in SM and Chol, such as those of enveloped viruses, as predicted by the biomolecular simulations (Figure 3).

We conclude that experiments on model membranes strongly support the suggested mechanism of membrane destabilization by supramolecular docking of designed ligands to the lipid head groups and subsequent increase in surface tension. Importantly, lipid rafts are enriched in viral membranes, which makes them more susceptible to disruption by tweezers. Indeed, a single rupture of the viral membrane destroys the virus irreversibly. By contrast, cells can actively repair their membranes after lipid-raft disruption.

CLR01 Induces Distortions in Viral Membrane. We next visualized the effect of the tweezers on the envelope of virus particles. We first analyzed HIV-1 and ZIKV by cryo-transmission electron microscopy (cryo-TEM) but encountered problems at detecting a sufficient number of the relatively small virions (data not shown). We therefore switched to HCMV, a relatively large virus, which is antagonized by CLR01.¹⁴ Cryo-TEM analysis of untreated HCMV virions showed ~ 200 nm-sized particles with a protein-rich tegument and an intact

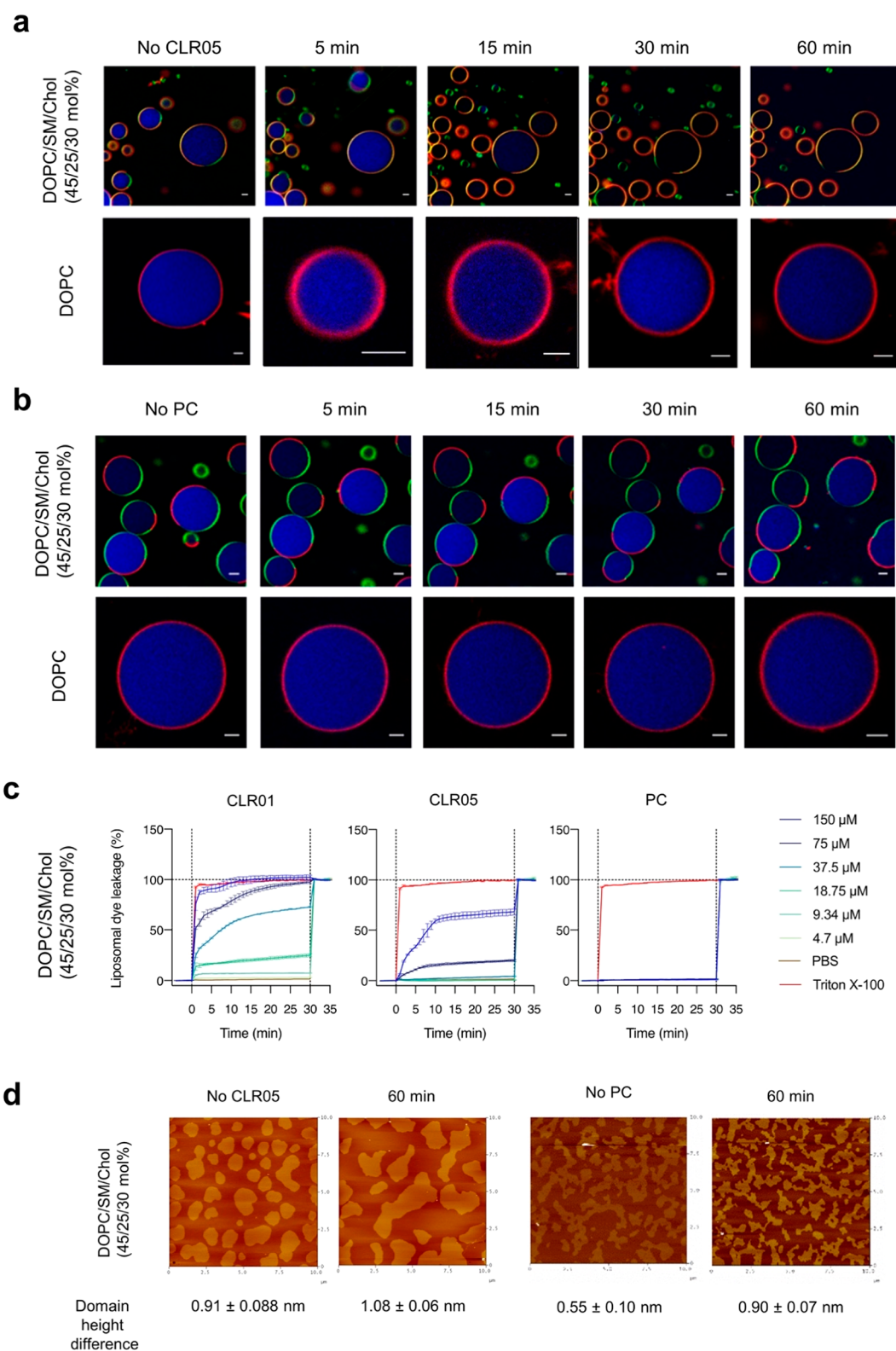


Figure 5. CLR05 destroys raft-like lipid vesicles. (a, b) Confocal fluorescence microscopy images of lipid raft enriched GUVs consisting of pure DOPC (lower panel) or a DOPC/SM/Chol (45/25/30 mol %) lipid mixture (upper panel) labeled with N-Rh-DHPE (l_d lipid phase, red channel) and Bodipy-Chol (l_o lipid phase, green channel) and filled with Atto 647 dye (blue channel). CLR05 (a) or PC (b) (150 μ M) was added and incubated for the indicated times. Scale bar: 5 μ m. (c) Liposome dye leakage assay of DOPC/SM/Chol (45/25/30 mol %) liposomes extruded to 200 nm size filled with 50 mM carboxyfluorescein. Compounds were added after measuring baseline fluorescence for 5 min (first dotted line), and after 30 min of incubation with compounds, Triton X-100 was added to 1% final concentration to measure fluorescence intensity after full leakage in each well (second dotted line). Fluorescence values were baseline-subtracted (before addition of compounds) and normalized to maximum fluorescence obtained after addition of Triton X-100. Values represent means \pm SD ($n = 3$). (d) AFM images of a DOPC/SM/Chol (45/25/30 mol %) lipid membrane on mica before injection (0 min) and after injection of 150 μ M CLR05 (left) or PC (right) in 10 mM NaH_2PO_4 , pH 7.6 into the AFM fluid cell.

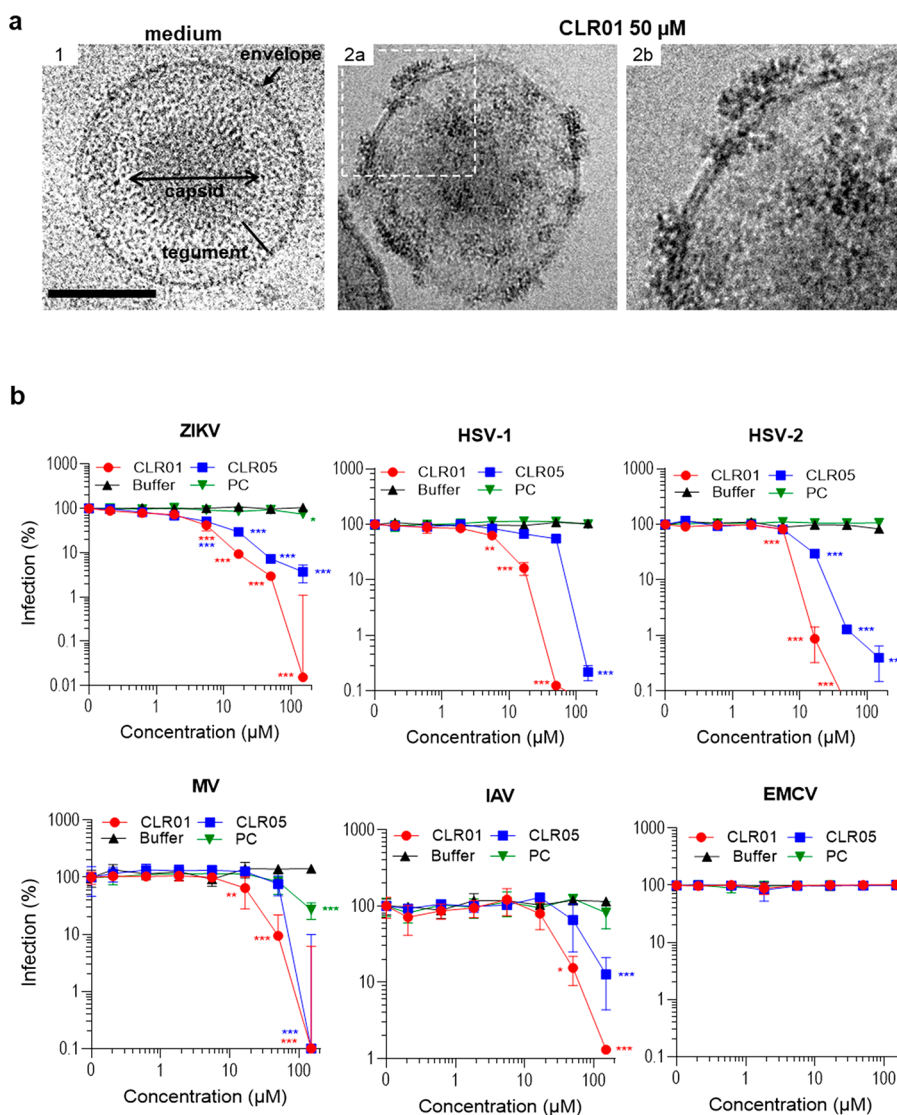


Figure 6. CLR01 destroys the HCMV envelope and exerts broad antiviral activity against enveloped virus infection. (a) Cryo-TEM of HCMV virions after treatment with medium (1) or 50 μM CLR01 (2a-b) for 30 min at 37 $^{\circ}\text{C}$. Important virion structures are indicated in image 1. CLR01-treated virion in 2a-b shows a discontinuous envelope and is decorated with electron-dense material at these sites (white arrowhead). Scale bar is 100 nm. (b) Antiviral activity of tweezers and clip against enveloped (ZIKV, HSV-1, HSV-2, HCMV, MV, IAV) and nonenveloped virus infection (EMCV). ZIKV MR766 was incubated for 30 min at 37 $^{\circ}\text{C}$ with buffer or 0.2–150 μM CLR01, CLR05, or PC before these mixtures were added to Vero E6 cells. After 2 dpi, cell-based ZIKV immunodetection was performed. Values represent means \pm SEM ($n = 3$). HSV-1 and HSV-2 were incubated for 30 min with compounds and then added to Vero E6 cells. After 1 h incubation, media were changed; 12 h post infection, cells were fixed, and infection rates were quantified via staining for the HSV protein ICP0. Values represent means of % infection \pm SD ($n = 3$). Measles virus was exposed to compounds for 30 min at 37 $^{\circ}\text{C}$ before these mixtures were added to A549 cells. After 4 h, cells were washed, and medium was replaced. After 2 dpi, infection rates were quantified by staining with an FITC-coupled MV antibody and mean fluorescence intensities were measured on a plate reader. Values represent means \pm SD ($n = 6$). Influenza strain A/PR/8/34 was incubated with 0–150 μM CLR01, CLR05, or PC for 30 min at 37 $^{\circ}\text{C}$ before the mixtures were used to infect A549 cells. After 1 h, cells were washed, and medium was changed. After 48 h, infectivity rates were determined by measuring neuraminidase activity in cellular lysates (MUNANA assay). Values represent means \pm SD ($n = 3$). EMCV was incubated for 30 min at 37 $^{\circ}\text{C}$ with buffer or different concentrations of CLR01, CLR05, or PC before it was added to HFF cells. Two days later, the cytopathic effect (percentage of detached cells) was quantified by MTT assay and used to calculate infection rates. Values represent means \pm SD ($n = 3$).

membrane in 78.1% of all analyzed images ($n = 32$) (Figure 6a, Supplementary Figure 8a and Supplementary Table 5). Upon incubation of HCMV with CLR01 for 30 min, we observed distortions in the viral membrane in 84.6% of the analyzed samples ($n = 39$) (Figure 6a, Supplementary Figure 8a and Supplementary Table 5). Interestingly, these distortions resulted in the leakage of the gel-like tegument to the outside of the virus, but not an entire loss of the structural integrity of the viral particle. Viral DNA release assays confirmed that CLR01 does not cause an entire destruction of the HCMV particle

(Supplementary Figure 8b). These data are in contrast to those obtained with HIV-1 and ZIKV,^{14,24} where CLR01 and CLR05 resulted in complete destruction of the virions (Supplementary Figure 9). However, this discrepancy is likely explained by the fact that HCMV is a relatively stable virus because of the numerous interactions of the viral glycoproteins with the tegument, explaining its partial resistance even against detergents (Supplementary Figure 8b). To assess whether CLR01 or CLR05 might induce virus aggregation, we utilized fluorescent nanoparticle tracking of virus-like particles. We did

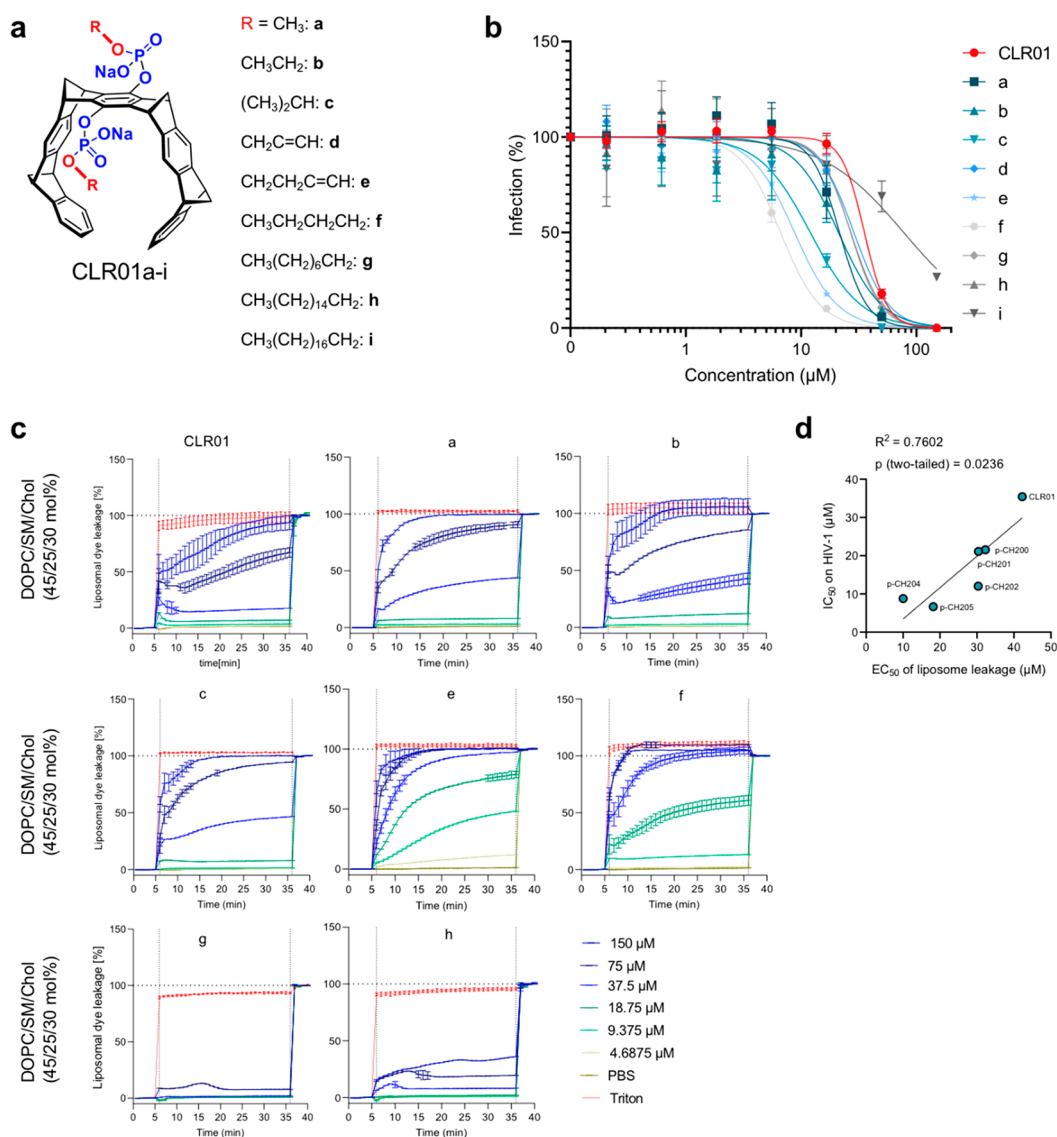


Figure 7. Advanced molecular tweezer derivatives with two aliphatic ester arms display improved activity against HIV-1 infection. (a) Chemical structures of the new two-armed tweezer derivatives developed from the parent phosphate tweezer CLR01. (b) Effect of the new tweezers on HIV-1 infection. HIV-1 was exposed to tweezer at indicated concentrations and then used to infect TZM-bl cells. Infection rates were determined 2 days later by quantifying β -galactosidase activity. Shown are mean values derived from 1–3 experiments each performed in triplicates \pm SEM. (c) Liposome dye leakage assay of DOPC/SM/Chol (45/25/30 mol %) liposomes filled with 50 mM carboxyfluorescein. Compounds were added after measuring baseline fluorescence for 5 min (first dotted line) and after 30 min incubation with compounds, Triton X-100 was added to 1% final concentration to measure fluorescence intensity after full leakage in each well (second dotted line). Fluorescence values were baseline-subtracted (before addition of compounds) and normalized to maximum fluorescence obtained after addition of Triton X-100. Values represent means \pm SD ($n = 3$). (d) Correlation of anti-HIV IC₅₀ values from (b) and EC₅₀ measured in the liposome leakage assays (c). Derivates g and h were excluded, as 50% leakage was not reached, and thus no EC₅₀ was calculated.

not see any aggregation of virus-like particles induced by CLR01, CLR03, CLR05, or PC (Supplementary Figure 10). By contrast, SEVI fibrils induced aggregation of viral particles as expected (Supplementary Figure 10). These findings suggest that CLR01 and CLR05 disrupt viral membranes without inducing aggregation of the virus.

CLR01 and CLR05 are Broad-Spectrum Antivirals. If tweezers act against viral membranes, they should be generally active against enveloped viruses. Indeed, we found that CLR05 abrogated infection of pseudoviruses carrying the glycoproteins of Marburg, Ebola, rabies, or SARS-coronavirus 1 (Supplementary Figure 11a), as previously shown for CLR01.²⁴ Moreover, we found that both tweezers inhibited infection by

pseudoviruses harboring the spike glycoprotein of SARS-CoV-2, the causative agent of the ongoing COVID-19 pandemic, whereas PC had a modest effect at high concentrations (Supplementary Figure 11b). CLR01 and CLR05 also inhibited infection of replication-competent ZIKV, HSV-1, HSV-2, measles virus (MV), and influenza virus (Figure 6b) with a mean IC₅₀ of 19.3 μ M for CLR01 and 38.1 μ M for CLR05. The clip did not affect infectivity of any of these viruses except for a modest effect on MV (Figure 6b). Importantly, neither CLR01 nor CLR05 reduced infection by nonenveloped adenovirus (Supplementary Figure 11c) or encephalomyocarditis virus (Figure 6b). Thus, our results indicate that CLR01 and CLR05 are both broad-spectrum inhibitors of pathogenic enveloped

viruses. We cannot exclude at this point that CLR01 binding to lysine-rich tracts of viral proteins may also influence virus attachment to the host cell and thereby decrease infectivity. However, the structure of these glycoproteins varies greatly between different viruses, and interference with protein interactions usually requires higher affinities than those displayed by CLR01 ($>20 \mu\text{M}$). Furthermore, electron microscopy demonstrates a direct destabilization of the viral envelope by CLR01 (Figure 6a).¹⁴ Indeed, there has so far been no exception from the empirical rule that molecular tweezers disrupt the membrane of all enveloped viruses but are inactive against nonenveloped viruses.

Additional Lipid Anchors Significantly Improve the Antiviral Activity of CLR01. If the mechanistic picture of membrane destabilization by direct tweezer docking onto lipid head groups is correct, additional lipid anchors on the tweezer should enhance this interaction and yield more potent scaffolds. In a first series of advanced tweezers, we introduced a wide range of aliphatic ester arms into each phosphate group of CLR01 (Figure 7a). These modifications were accomplished by activation of the phosphoric acid with trichloroacetone (TCA), which can be controlled in pyridine to occur only once.¹⁴ The length of these additional lipid anchors was varied between C1 and C16 chains, and initial antiviral activities were assessed with the same experiments on HIV-1 as described for CLR01, CLR05, and PC. Intriguingly, most tweezer derivatives are more effective than their parent compound CLR01 (Figure 7b). The most efficient esters carried unbranched C4 units (CLR01-e and -f) and inhibit HIV-1 infection at ~ 4 – 5 -fold lower concentrations than CLR01. The CLR01 analogue with C18 chains, CLR01-i, was highly cytotoxic (Figure 7b and Supplementary Figure 12). The selectivity index of the modified tweezers confirmed that the advanced tweezers with lipid anchors, in particular CLR01-e and -f, are indeed superior to their ancestor CLR01 (Supplementary Figure 12b). The only exception was CLR01-i, which was cytotoxic (Supplementary Figure 12b). Liposomal dye-leakage assays demonstrated that most CLR01 derivatives induced a more rapid and more effective membrane disruption than the parent CLR01 (Figure 7c, Supplementary Figure 7d). Moreover, we observed a statistically significant ($p < 0.05$) correlation between the anti-HIV activity and potency in liposome disruption, supporting the above-detailed mechanism (Figure 7d). These findings show one way for improving efficacy of tweezers, namely by the introduction of membrane-active components to the parent tweezer unit. We are now performing a broad screening of such modified tweezers to identify powerful nontoxic candidates.

DISCUSSION

The molecular tweezer CLR01 is a well-established inhibitor of abnormal protein self-assembly and has been found to inhibit the formation of toxic oligomers and aggregates of multiple disease-associated proteins, including those involved in Alzheimer's disease^{38,39} and Parkinson's disease.^{10,40,41} Moreover, CLR01 also blocks formation of seminal amyloid fibrils¹⁴ that are potent enhancers of Ebola virus and HIV-1 infection.^{15,21} The anti-amyloid activity is achieved by reversible inclusion of positively charged amino acid residues inside the tweezer cavity, primarily Lys and to a lower extent Arg.¹⁴ More recently, we demonstrated that CLR01 also acts as broad-spectrum inhibitor of enveloped viruses, including HIV-1, ZIKV and Ebola virus.²⁴ The exact mechanism underlying the antiviral activity of CLR01 was, however, unclear.

We show here that the anti-amyloid and the antiviral activity are separable functions of CLR01. CLR05, a tweezer derivative that carries methylene carboxylates instead of phosphates, does not encapsulate Lys/Arg residues and consequently displays no anti-amyloid activity. However, like CLR01, CLR05 suppresses virus infection in a dose-dependent manner. This finding demonstrates that Lys/Arg inclusion is not necessary for virus inhibition. On the other hand, the phosphate clip PC, a structurally related phosphorylated derivative with a modified open cavity, was devoid of both activities, indicating that the closed horseshoe-shaped cavity of the tweezers plays a key role in viral membrane destabilization by CLR01 and CLR05. In agreement with these results, only CLR01, but not CLR05 and PC, effectively prevented complex formation between seminal fibrils and virions, and abrogated infectivity-enhancement. We conclude that the anti-amyloid activity relies on Lys/Arg inclusion inside the tweezer cavity. This inclusion leads to a neutralized zeta potential of the fibrils, and eliminates their potential to carry virions to the cell membrane.

How do CLR01 and CLR05 destabilize and eventually disrupt the viral membrane? Through a combination of biomolecular simulations, model titrations (¹H NMR, fluorescence) and liposome experiments, we discovered that CLR01, CLR05, and PC all engage lipid head groups at the surface of biological and synthetic membranes. This supramolecular process involves encapsulation of the trimethylammonium moiety of the choline of DOPC or SM inside the cavities of the ligands, which only occurs close to the membrane surface. Here, even the amphiphilic CLR05 orients its methylene carboxylate arms toward the bulk water and thus exposes its cavity. Antiviral tweezers CLR01 and CLR05 induce a horizontal lipid orientation inside their closed cavities, which favors their insertion in the polar region of the outer leaflet and raises the local stress of the membrane. This rearrangement ultimately ruptures viral membranes—as visualized by cryo-TEM of CLR01-exposed HCMV particles—and diminishes viral infectivity. By contrast, the open PC cavity allows stress-free lipid insertion from below and hence does not affect viral membrane integrity, explaining the lack of antiviral activity.

Experiments with fluorescent GUVs and liposomes suggest a profound difference between DOPC membranes, which remain intact after tweezer or clip exposure, and DOPC liposomes containing SM and Chol, which imitate the composition of viral membranes and are quickly disrupted at their phase boundaries between DOPC and lipid rafts when tweezers are added. We explain this difference by the elevated surface tension already present in lipid rafts, which is further increased after CLR01 or CLR05 insertion. Our findings also explain the minimal cytotoxicity of tweezers¹⁴ because the surface tension of the ordinary cellular plasma membrane is much lower than that of small nanometer-sized liposomal or viral membranes, which are disrupted by CLR01 or CLR05. In addition, we show by QM/MM calculations and NMR experiments that the inclusion complexes with SM are intrinsically more stable than those with DOPC, which is rationalized by a reduced competition between electrostatic and dispersion forces and solvation effects in SM.

CLR01 showed a modestly increased antiviral activity as compared to CLR05. Leakage assays revealed that CLR01 lyses DOPC/SM/Chol liposomes more rapidly and more effectively than CLR05. Computational modeling and NMR titrations showed that CLR05 is able to bind the trimethylammonium cation of the choline head group also outside the cavity by way of a chelate complex between its carboxylate tips. This binding

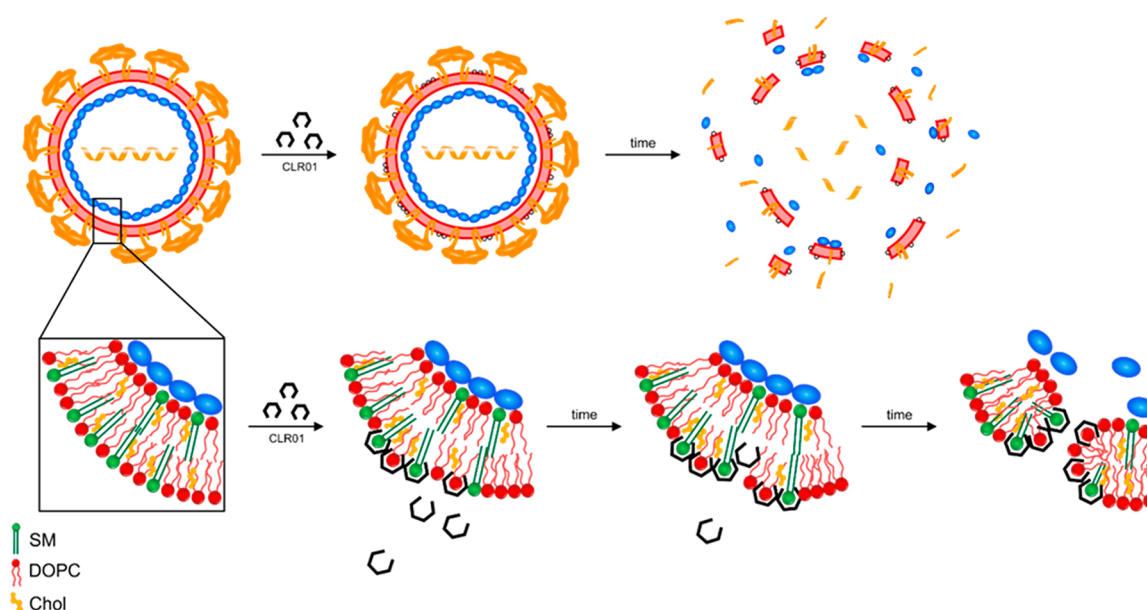


Figure 8. Schematic representation of virus disruption by molecular tweezers. Tweezer molecules encapsulate the phosphocholine head groups of DOPC and SM in the outer lipid leaflet of the viral membrane, thereby increasing the mechanical stress in the outer leaflet, which initiates the rupture of the viral membrane and consequently loss of viral infectivity.

mode is weaker, does not exert any strain on the lipids inside the membrane, and thus lowers the membrane destabilization efficiency. Collectively, these data suggest that tweezer architecture and the direct inclusion of the choline head group inside the tweezer cavity are required for their biological effect. Importantly, additional lipid anchor groups on the phosphate moieties further strengthen this effect (Figure 7).

We also observed that some viruses need a larger amount of tweezers than others in order to be disrupted. For example, CLR01 was more effective against HSV-2 than IAV (Figure 6b). This difference could be caused by distinct capsid/envelope packaging of various viruses, the overall virion architecture, the membrane curvature and/or tension, or the accessibility of the viral membrane because of the incorporation of viral and cellular proteins. Another explanation is that the total number of infectious, subinfectious, or noninfectious particles as well as the absolute infectious titer can vary greatly between different stocks of the same virus and even more between different virus families. In the light of these differences, it is actually surprising that all IC_{50} values determined so far (in independent studies with different viruses) were always between 5 and 50 μM .^{14,24} These findings further underline the proposed universal antiviral mode of action: the direct interaction and disruption of the viral membrane by the tweezer. The micromolar IC_{50} values may reflect the large number of lipids in the membrane which must be occupied by molecular tweezers before rupture occurs. An indication for this possibility comes from elevated IC_{50} levels observed when viral preparations contain large amounts of cellular fragments (data not shown). However, CLR01 binds very weakly to choline head groups (mM K_d range) and in a fully reversible manner with fast exchange (averaged NMR signals). Only when the surface tension exceeds the critical threshold is the viral membrane disrupted irreversibly.

In conclusion, CLR01 and CLR05 specifically target enveloped viruses by destroying the integrity of the viral membrane (Figure 8). Both tweezers do not affect “naked” EMCV or adenovirus infection but are active against all analyzed enveloped viruses, including not only well-known pathogens

such as herpesviruses or HIV-1 but also emerging or reemerging viruses, including Ebola and Zika virus. A series of two-armed new tweezers was synthesized based on this mechanistic insight, which display significantly improved antiviral activities. Their additional lipid anchors increase viral membrane destabilization, and opens the path for structural optimization to more potent scaffolds. Our findings may be particularly useful for prevention and treatment of viruses, where no specific antiviral therapy exists as with the ongoing SARS-CoV-2/COVID-19 pandemic. Moreover, the apparent lack of toxicity in animal models render molecular tweezers very promising lead compounds for a novel class of potential broad-spectrum antivirals.^{40,42–46}

Safety. To the best of our knowledge, there are no unexpected, new, or significant hazards or risks associated with the reported work.

■ ASSOCIATED CONTENT

Supporting Information

This material is available free of charge on the ACS Web site (<https://pubs.acs.org/doi/10.1021/jacs.0c06400>). The Supporting Information is available free of charge at <https://pubs.acs.org/doi/10.1021/jacs.0c06400>.

Materials and methods, supplementary figures and tables, and references of materials and methods (PDF)

■ AUTHOR INFORMATION

Corresponding Authors

Jan Münch – Institute of Molecular Virology, Ulm University Medical Center, 89081 Ulm, Germany; orcid.org/0000-0001-7316-7141; Email: jan.muench@uni-ulm.de

Elsa Sanchez-Garcia – Computational Biochemistry, Center of Medical Biotechnology, University of Duisburg-Essen, 45117 Essen, Germany; orcid.org/0000-0002-9211-5803; Email: elsa.sanchez-garcia@uni-due.de

James Shorter – Cell and Molecular Biology Graduate Group and Department of Biochemistry and Biophysics, Perelman School of Medicine at the University of Pennsylvania, Philadelphia,

Pennsylvania 19104, United States; orcid.org/0000-0001-5269-8533; Email: jshorter@penndu.upenn.edu

Thomas Schrader – Faculty of Chemistry, University of Duisburg-Essen, 45117 Essen, Germany; orcid.org/0000-0002-7003-6362; Email: thomas.schrader@uni-due.de

Authors

Tatjana Weil – Institute of Molecular Virology, Ulm University Medical Center, 89081 Ulm, Germany; orcid.org/0000-0003-0925-2426

Rüdiger Groß – Institute of Molecular Virology, Ulm University Medical Center, 89081 Ulm, Germany

Annika Röcker – Institute of Molecular Virology, Ulm University Medical Center, 89081 Ulm, Germany

Kenny Bravo-Rodriguez – Computational Biochemistry, Center of Medical Biotechnology, University of Duisburg-Essen, 45117 Essen, Germany

Christian Heid – Faculty of Chemistry, University of Duisburg-Essen, 45117 Essen, Germany

Andrea Sowislok – Faculty of Chemistry, University of Duisburg-Essen, 45117 Essen, Germany

My-Hue Le – Faculty of Chemistry, University of Duisburg-Essen, 45117 Essen, Germany

Nelli Erwin – Physical Chemistry I–Biophysical Chemistry, Faculty of Chemistry and Chemical Biology, TU Dortmund University, 44227 Dortmund, Germany

Mridula Dwivedi – Physical Chemistry I–Biophysical Chemistry, Faculty of Chemistry and Chemical Biology, TU Dortmund University, 44227 Dortmund, Germany

Stephen M. Bart – Department of Microbiology and Cell and Molecular Biology Graduate Group, Perelman School of Medicine at the University of Pennsylvania, Philadelphia, Pennsylvania 19104, United States

Paul Bates – Department of Microbiology and Cell and Molecular Biology Graduate Group, Perelman School of Medicine at the University of Pennsylvania, Philadelphia, Pennsylvania 19104, United States

Lukas Wettstein – Institute of Molecular Virology, Ulm University Medical Center, 89081 Ulm, Germany

Janis A. Müller – Institute of Molecular Virology, Ulm University Medical Center, 89081 Ulm, Germany

Mirja Harms – Institute of Molecular Virology, Ulm University Medical Center, 89081 Ulm, Germany

Konstantin Sparrer – Institute of Molecular Virology, Ulm University Medical Center, 89081 Ulm, Germany

Yasser B. Ruiz-Blanco – Computational Biochemistry, Center of Medical Biotechnology, University of Duisburg-Essen, 45117 Essen, Germany; orcid.org/0000-0001-5400-4427

Christina M. Stürzel – Institute of Molecular Virology, Ulm University Medical Center, 89081 Ulm, Germany

Jens von Einem – Institute of Virology, Ulm University Medical Center, 89081 Ulm, Germany

Sina Lippold – Institute of Virology, Ulm University Medical Center, 89081 Ulm, Germany

Clarissa Read – Institute of Virology, Ulm University Medical Center, 89081 Ulm, Germany; Central Facility for Electron Microscopy, Ulm University, 89081 Ulm, Germany

Paul Walther – Central Facility for Electron Microscopy, Ulm University, 89081 Ulm, Germany

Marco Hebel – Max Planck Institute for Polymer Research, 55128 Mainz, Germany; Institute of Inorganic Chemistry I, Ulm University, 89081 Ulm, Germany

Florian Kreppel – Center for Biomedical Education and Research, University of Witten/Herdecke, 58453 Witten, Germany

Frank-Gerrit Klärner – Faculty of Chemistry, University of Duisburg-Essen, 45117 Essen, Germany

Gal Bitan – Department of Neurology, David Geffen School of Medicine, Brain Research Institute, and Molecular Biology Institute, University of California, Los Angeles, Los Angeles, California 90095, United States; orcid.org/0000-0001-7046-3754

Michael Ehrmann – Microbiology II, Center of Medical Biotechnology, University of Duisburg-Essen, 45117 Essen, Germany; orcid.org/0000-0002-1927-260X

Tanja Weil – Max Planck Institute for Polymer Research, 55128 Mainz, Germany; Institute of Inorganic Chemistry I, Ulm University, 89081 Ulm, Germany; orcid.org/0000-0002-5906-7205

Roland Winter – Physical Chemistry I–Biophysical Chemistry, Faculty of Chemistry and Chemical Biology, TU Dortmund University, 44227 Dortmund, Germany; orcid.org/0000-0002-3512-6928

Complete contact information is available at: <https://pubs.acs.org/10.1021/jacs.0c06400>

Author Contributions

▲T.W., R.G., A.R., and K.B.-R. contributed equally.

Notes

All data were analyzed using GraphPad Prism version 7.03 for Windows, GraphPad Software, La Jolla California USA (www.graphpad.com). Significance levels were calculated using one-way analysis of variance (ANOVA) (nonparametric, grouped), followed by Bonferroni's or Dunnett's multiple comparison test (indicated in figure legends). *p*-Values of <0.01 were considered significant (*, *p* < 0.01 **, *p* < 0.001 ***, *p* < 0.0001). In some cases, unpaired *t* tests (parametric, two-tailed) were used to compare a buffer control to compound-treated conditions.

The authors declare the following competing financial interest(s): A.R., C.H., A.S., T.S., G.B., and J.M. are inventors on the provisional patent application 62/692,479 New Molecular Tweezers against Neurological Disorders and Viral Infections. J.S. is a consultant for Dewpoint Therapeutics.

ACKNOWLEDGMENTS

M.H., T.W., L.W. and R.G. are part of the International Graduate School in Molecular Medicine Ulm. R.G. was funded by a scholarship from the International Graduate School in Molecular Medicine Ulm. P.W., J.M., and E.S.-G. acknowledge funding by the DFG CRC1279. J.S. was supported by a Bill and Melinda Gates Foundation Grand Challenges Explorations Award and NIH grant R21HD074510. J.M. acknowledges funding by the Volkswagen Foundation and the EU's Horizon 2020 research and innovation programme (Fight-nCoV, 101003555). J.A.M. is funded by a grant from the Medical Faculty of Ulm University and indebted to the Baden-Württemberg Stiftung for the financial support of this research project by the Eliteprogramme for Postdocs. A.S., C.H., and T.S. as well as K.B.R. and E.S.-G. gratefully acknowledge funding by the DFG CRC 1093 "Supramolecular Chemistry on Proteins" (A3 and A8). E.S.-G. and R.W. acknowledge the Deutsche Forschungsgemeinschaft (DFG, German Research Foundation) under Germany's Federal and State Excellence Strategy EXC-2033 Projektnummer 390677874. E.S.-G. also acknowledges the Boehringer Ingelheim Foundation (Plus-3 grant) and the

computational time provided by the Computing and Data Facility of the Max Planck Society and the supercomputer magnetUDE of the University of Duisburg-Essen. G.B. acknowledges support from NIH/NIA grant R01AG050721. We thank Stefan Pöhlmann for providing the SARS-CoV-2 spike expression plasmid.

REFERENCES

(1) Jackman, J. A.; Shi, P. Y.; Cho, N. J. Targeting the Achilles Heel of Mosquito-Borne Viruses for Antiviral Therapy. *ACS Infect. Dis.* **2019**, *5* (1), 4–8.

(2) Vigant, F.; Santos, N. C.; Lee, B. Broad-Spectrum Antivirals against Viral Fusion. *Nature Reviews Microbiology*; Nature Publishing Group: 2015; pp 426–437.

(3) Liao, M.; Kielian, M. Domain III from Class II Fusion Proteins Functions as a Dominant-Negative Inhibitor of Virus Membrane Fusion. *J. Cell Biol.* **2005**, *171* (1), 111–120.

(4) Koehler, J. W.; Smith, J. M.; Ripoll, D. R.; Spik, K. W.; Taylor, S. L.; Badger, C. V.; Grant, R. J.; Ogg, M. M.; Wallqvist, A.; Guttieri, M. C.; Garry, R. F.; Schmaljohn, C. S. A Fusion-Inhibiting Peptide against Rift Valley Fever Virus Inhibits Multiple, Diverse Viruses. *PLoS Neglected Trop. Dis.* **2013**, *7* (9), e2430.

(5) Diwaker, D.; Mishra, K. P.; Ganju, L. Potential Roles of Protein Disulphide Isomerase in Viral Infections. *Acta Virol.* **2013**, *57* (3), 293–304.

(6) Badani, H.; Garry, R. F.; Wimley, W. C. Peptide Entry Inhibitors of Enveloped Viruses: The Importance of Interfacial Hydrophobicity. *Biochim. Biophys. Acta, Biomembr.* **2014**, *1838*, 2180–2197.

(7) Pollock, S.; Nichita, N. B.; Bohmer, A.; Radulescu, C.; Dwek, R. A.; Zitzmann, N. Polyunsaturated Liposomes Are Antiviral against Hepatitis B and C Viruses and HIV by Decreasing Cholesterol Levels in Infected Cells. *Proc. Natl. Acad. Sci. U. S. A.* **2010**, *107* (40), 17176–17181.

(8) St. Vincent, M. R.; Colpitts, C. C.; Ustinov, A. V.; Muqadas, M.; Joyce, M. A.; Barsby, N. L.; Epan, R. F.; Epan, R. M.; Khramyshev, S. A.; Valueva, O. A.; Korshun, V. A.; Tyrrell, D. L. J.; Schang, L. M. Rigid Amphipathic Fusion Inhibitors, Small Molecule Antiviral Compounds against Enveloped Viruses. *Proc. Natl. Acad. Sci. U. S. A.* **2010**, *107* (40), 17339–17344.

(9) Hollmann, A.; Castanho, M. A. R. B.; Lee, B.; Santos, N. C. Singlet Oxygen Effects on Lipid Membranes: Implications for the Mechanism of Action of Broad-Spectrum Viral Fusion Inhibitors. *Biochem. J.* **2014**, *459* (1), 161–170.

(10) Sinha, S.; Lopes, D. H. J.; Du, Z.; Pang, E. S.; Shanmugam, A.; Lomakin, A.; Talbiersky, P.; Tennstaedt, A.; McDaniel, K.; Bakshi, R.; Kuo, P. Y.; Ehrmann, M.; Benedek, G. B.; Loo, J. A.; Klärner, F. G.; Schrader, T.; Wang, C.; Bitan, G. Lysine-Specific Molecular Tweezers Are Broad-Spectrum Inhibitors of Assembly and Toxicity of Amyloid Proteins. *J. Am. Chem. Soc.* **2011**, *133* (42), 16958–16969.

(11) Attar, A.; Bitan, G. Disrupting Self-Assembly and Toxicity of Amyloidogenic Protein Oligomers by “Molecular Tweezers” - from the Test Tube to Animal Models. *Curr. Pharm. Des.* **2014**, *20* (15), 2469–2483.

(12) Schrader, T.; Bitan, G.; Klärner, F. G. Molecular Tweezers for Lysine and Arginine-Powerful Inhibitors of Pathologic Protein Aggregation. *Chem. Commun.* **2016**, *52* (76), 11318–11334.

(13) Hadrovic, I.; Rebmann, P.; Klärner, F.-G.; Bitan, G.; Schrader, T. Molecular Lysine Tweezers Counteract Aberrant Protein Aggregation. *Front. Chem.* **2019**, *7*, 657.

(14) Lump, E.; Castellano, L. M.; Meier, C.; Seeliger, J.; Erwin, N.; Sperlich, B.; Stürzel, C. M.; Usmani, S.; Hammond, R. M.; Von Einem, J.; Gerold, G.; Kreppel, F.; Bravo-Rodriguez, K.; Pietschmann, T.; Holmes, V. M.; Palesch, D.; Zirafi, O.; Weissman, D.; Sowislok, A.; Wettig, B.; Heid, C.; Kirchhoff, F.; Weil, T.; Klärner, F. G.; Schrader, T.; Bitan, G.; Sanchez-Garcia, E.; Winter, R.; Shorter, J.; Munch, J. A Molecular Tweezer Antagonizes Seminal Amyloids and HIV Infection. *eLife* **2015**, *4* (August), 1–33.

(15) Münch, J.; Rücker, E.; Ständker, L.; Adermann, K.; Goffinet, C.; Schindler, M.; Wildum, S.; Chinnadurai, R.; Rajan, D.; Specht, A.; Giménez-Gallego, G.; Sánchez, P. C.; Fowler, D. M.; Koulov, A.; Kelly, J. W.; Mothes, W.; Grivel, J. C.; Margolis, L.; Keppler, O. T.; Forssmann, W. G.; Kirchhoff, F. Semen-Derived Amyloid Fibrils Drastically Enhance HIV Infection. *Cell* **2007**, *131* (6), 1059–1071.

(16) Roan, N. R.; Müller, J. A.; Liu, H.; Chu, S.; Arnold, F.; Stürzel, C. M.; Walther, P.; Dong, M.; Witkowska, H. E.; Kirchhoff, F.; Münch, J.; Greene, W. C. Peptides Released by Physiological Cleavage of Semen Coagulum Proteins Form Amyloids That Enhance HIV Infection. *Cell Host Microbe* **2011**, *10* (6), 541–550.

(17) Usmani, S. M.; Zirafi, O.; Müller, J. A.; Sandi-Monroy, N. L.; Yadav, J. K.; Meier, C.; Weil, T.; Roan, N. R.; Greene, W. C.; Walther, P.; Nilsson, K. P. R.; Hammarström, P.; Wetzel, R.; Pilcher, C. D.; Gagsteiger, F.; Fändrich, M.; Kirchhoff, F.; Münch, J. Direct Visualization of HIV-Enhancing Endogenous Amyloid Fibrils in Human Semen. *Nat. Commun.* **2014**, *5* (1), 3508.

(18) Kim, K. A.; Yolamanova, M.; Zirafi, O.; Roan, N. R.; Staendker, L.; Forssmann, W. G.; Burgener, A.; Dejuq-Rainsford, N.; Hahn, B. H.; Shaw, G. M.; Greene, W. C.; Kirchhoff, F.; Münch, J. Semen-Mediated Enhancement of HIV Infection Is Donor-Dependent and Correlates with the Levels of SEVI. *Retrovirology* **2010**, *7* (1), 55.

(19) Castellano, L. M.; Shorter, J. The Surprising Role of Amyloid Fibrils in HIV Infection. *Biology* **2012**, 58–80.

(20) Torres, L.; Ortiz, T.; Tang, Q. Enhancement of Herpes Simplex Virus (HSV) Infection by Seminal Plasma and Semen Amyloids Implicates a New Target for the Prevention of HSV Infection. *Viruses* **2015**, *7* (4), 2057–2073.

(21) Bart, S. M.; Cohen, C.; Dye, J. M.; Shorter, J.; Bates, P. Enhancement of Ebola Virus Infection by Seminal Amyloid Fibrils. *Proc. Natl. Acad. Sci. U. S. A.* **2018**, *115* (28), 7410–7415.

(22) Roan, N. R.; Munch, J.; Arhel, N.; Mothes, W.; Neidleman, J.; Kobayashi, A.; Smith-McCune, K.; Kirchhoff, F.; Greene, W. C. The Cationic Properties of SEVI Underlie Its Ability To Enhance Human Immunodeficiency Virus Infection. *J. Virol.* **2009**, *83* (1), 73–80.

(23) Arnold, F.; Schnell, J.; Zirafi, O.; Stürzel, C.; Meier, C.; Weil, T.; Ständker, L.; Forssmann, W.-G.; Roan, N. R.; Greene, W. C.; Kirchhoff, F.; Munch, J. Naturally Occurring Fragments from Two Distinct Regions of the Prostatic Acid Phosphatase Form Amyloidogenic Enhancers of HIV Infection. *J. Virol.* **2012**, *86* (2), 1244–1249.

(24) Röcker, A. E.; Müller, J. A.; Dietzel, E.; Harms, M.; Krüger, F.; Heid, C.; Sowislok, A.; Riber, C. F.; Kupke, A.; Lippold, S.; von Einem, J.; Beer, J.; Knöll, B.; Becker, S.; Schmidt-Chanasit, J.; Otto, M.; Vapalahti, O.; Zelikin, A. N.; Bitan, G.; Schrader, T.; Münch, J. The Molecular Tweezer CLR01 Inhibits Ebola and Zika Virus Infection. *Antiviral Res.* **2018**, *152*, 26–35.

(25) Dutt, S.; Wilch, C.; Gersthagen, T.; Talbiersky, P.; Bravo-Rodriguez, K.; Hanni, M.; Sánchez-García, E.; Ochsenfeld, C.; Klärner, F. G.; Schrader, T. Molecular Tweezers with Varying Anions: A Comparative Study. *J. Org. Chem.* **2013**, *78* (13), 6721–6734.

(26) Talbiersky, P.; Bastkowski, F.; Klärner, F. G.; Schrader, T. Molecular Clip and Tweezer Introduce New Mechanisms of Enzyme Inhibition. *J. Am. Chem. Soc.* **2008**, *130* (30), 9824–9828.

(27) Polkowska, J.; Bastkowski, F.; Schrader, T.; Klärner, F.-G.; Zienau, J.; Koziol, F.; Ochsenfeld, C. A Combined Experimental and Theoretical Study of the PH-Dependent Binding Mode of NAD⁺ by Water-Soluble Molecular Clips. *J. Phys. Org. Chem.* **2009**, *22* (8), 779–790.

(28) Jasper, C.; Schrader, T.; Panitzky, J.; Klärner, F.-G. Selective Complexation of N-Alkylpyridinium Salts: Recognition of NAD⁺ in Water. *Angew. Chem., Int. Ed.* **2002**, *41* (8), 1355–1358.

(29) Schrader, T.; Fokkens, M.; Klärner, F.-G.; Polkowska, J.; Bastkowski, F. Inclusion of Thiamine Diphosphate and S-Adenosylmethionine at Their Chemically Active Sites. *J. Org. Chem.* **2005**, *70* (25), 10227–10237.

(30) French, K. C.; Makhatazde, G. I. Core Sequence of Papf39 Amyloid Fibrils and Mechanism of Ph-Dependent Fibril Formation: The Role of Monomer Conformation. *Biochemistry* **2012**, *51* (51), 10127–10136.

(31) Lorizate, M.; Sachsenheimer, T.; Glass, B.; Habermann, A.; Gerl, M. J.; Kräusslich, H. G.; Brügger, B. Comparative Lipidomics Analysis of HIV-1 Particles and Their Producer Cell Membrane in Different Cell Lines. *Cell. Microbiol.* **2013**, *15* (2), 292–304.

(32) Thaa, B.; Siche, S.; Herrmann, A.; Veit, M. Acylation and Cholesterol Binding Are Not Required for Targeting of Influenza A Virus M2 Protein to the Hemagglutinin-Defined Budozone. *FEBS Lett.* **2014**, *588* (6), 1031–1036.

(33) Takahashi, T.; Suzuki, T. Function of Membrane Rafts in Viral Lifecycles and Host Cellular Response. *Biochem. Res. Int.* **2011**, *2011*, 1.

(34) Bavari, S.; Bosio, C. M.; Wiegand, E.; Ruthel, G.; Will, A. B.; Geisbert, T. W.; Hevey, M.; Schmaljohn, C.; Schmaljohn, A.; Javad Aman, M. Lipid Raft Microdomains: A Gateway for Compartmentalized Trafficking of Ebola and Marburg Viruses. *J. Exp. Med.* **2002**, *195* (5), 593–602.

(35) Brügger, B.; Glass, B.; Haberkant, P.; Leibrecht, I.; Wieland, F. T.; Kräusslich, H. G. The HIV Lipidome: A Raft with an Unusual Composition. *Proc. Natl. Acad. Sci. U. S. A.* **2006**, *103* (8), 2641–2646.

(36) Chan, R.; Uchil, P. D.; Jin, J.; Shui, G.; Ott, D. E.; Mothes, W.; Wenk, M. R. Retroviruses Human Immunodeficiency Virus and Murine Leukemia Virus Are Enriched in Phosphoinositides. *J. Virol.* **2008**, *82* (22), 11228–11238.

(37) Van Genderen, I. L.; Brandimarti, R.; Torrisi, M. R.; Campadelli, G.; Van Meer, G. The Phospholipid Composition of Extracellular Herpes Simplex Virions Differs from That of Host Cell Nuclei. *Virology* **1994**, *200* (2), 831–836.

(38) Sinha, S.; Du, Z.; Maiti, P.; Klärner, F. G.; Schrader, T.; Wang, C.; Bitan, G. Comparison of Three Amyloid Assembly Inhibitors: The Sugar Scyllo-Inositol, the Polyphenol Epigallocatechin Gallate, and the Molecular Tweezer CLR01. *ACS Chem. Neurosci.* **2012**, *3* (6), 451–458.

(39) Zheng, X.; Liu, D.; Klärner, F. G.; Schrader, T.; Bitan, G.; Bowers, M. T. Amyloid β -Protein Assembly: The Effect of Molecular Tweezers CLR01 and CLR03. *J. Phys. Chem. B* **2015**, *119* (14), 4831–4841.

(40) Prabhudesai, S.; Sinha, S.; Attar, A.; Kotagiri, A.; Fitzmaurice, A. G.; Lakshmanan, R.; Ivanova, M. I.; Loo, J. A.; Klärner, F. G.; Schrader, T.; Stahl, M.; Bitan, G.; Bronstein, J. M. A Novel “Molecular Tweezer” Inhibitor of α -Synuclein Neurotoxicity in Vitro and in Vivo. *Neurotherapeutics* **2012**, *9* (2), 464–476.

(41) Acharya, S.; Lapidus, L. J.; Safaie, B. M.; Attar, A.; Bitan, G.; Wongkongkathep, P.; Loo, J. A.; Ivanova, M. I.; Klärner, F.-G.; Schrader, T. Molecular Basis for Preventing α -Synuclein Aggregation by a Molecular Tweezer. *J. Biol. Chem.* **2014**, *289* (15), 10727–10737.

(42) Attar, A.; Chan, W. T. C.; Klärner, F. G.; Schrader, T.; Bitan, G. Safety and Pharmacological Characterization of the Molecular Tweezer CLR01-A Broad-Spectrum Inhibitor of Amyloid Proteins' Toxicity. *BMC Pharmacol. Toxicol.* **2014**, *15* (1), 23.

(43) Attar, A.; Ripoli, C.; Riccardi, E.; Maiti, P.; Li Puma, D. D.; Liu, T.; Hayes, J.; Jones, M. R.; Lichti-Kaiser, K.; Yang, F.; Gale, G. D.; Tseng, C. -h.; Tan, M.; Xie, C.-W.; Straudinger, J. L.; Klärner, F.-G.; Schrader, T.; Frautschy, S. A.; Grassi, C.; Bitan, G. Protection of Primary Neurons and Mouse Brain from Alzheimer's Pathology by Molecular Tweezers. *Brain* **2012**, *135* (12), 3735–3748.

(44) Ferreira, N.; Pereira-Henriques, A.; Attar, A.; Klärner, F. G.; Schrader, T.; Bitan, G.; Gales, L.; Saraiva, M. J.; Almeida, M. R. Molecular Tweezers Targeting Transthyretin Amyloidosis. *Neurotherapeutics* **2014**, *11* (2), 450–461.

(45) Fogerson, S. M.; van Brummen, A. J.; Busch, D. J.; Allen, S. R.; Roychaudhuri, R.; Banks, S. M. L.; Klärner, F. G.; Schrader, T.; Bitan, G.; Morgan, J. R. Reducing Synuclein Accumulation Improves Neuronal Survival after Spinal Cord Injury. *Exp. Neurol.* **2016**, *278*, 105–115.

(46) Lulla, A.; Barnhill, L.; Bitan, G.; Ivanova, M. I.; Nguyen, B.; O'Donnell, K.; Stahl, M. C.; Yamashiro, C.; Klärner, F. G.; Schrader, T.; Sagasti, A.; Bronstein, J. M. Neurotoxicity of the Parkinson Disease-Associated Pesticide Ziram Is Synuclein-Dependent in Zebrafish Embryos. *Environ. Health Perspect.* **2016**, *124* (11), 1766–1775.